Thermal Recycling of Bentonite Waste as a Novel and a Low-Cost Adsorbent for Heavy Metals Removal

Mukhtar D.H. Shubber[1], Daryoush Yousefi Kebria[1*]

[1] Department of Environmental Engineering, Civil Engineering Faculty, Babol Noshirvani University Of Technology, Babol, Iran

* Corresponding author's e-mail: dy.kebria@nit.ac.ir

ABSTRACT

The objectives of this study are the thermal remediation of bentonite waste to convert non-hazardous material, and the use of the obtainedthermal recycling bentonite waste (TRBW) as a novel low-cost adsorbent for the removal of heavy metals from aqueous solution using the batch system. The origin of bentonite waste is a by-product from plants of spent engine oil recycling [PSEOR]. It was remediated in two stages, directly burning and in the electrical furnace at 700 °C for 100 minutes to eliminate oil residues and impurities. The tests of XRD, BET, FTIR, EDX, and SEM were accomplished to identify the chemical and physical characteristics of TRBW. After then, the examination of the ability of TRBW to adsorption of the fiveheavy metals (Zn, Ni, Cd, Cr, and Pb) with different experimental parameters such as initial concentration, adsorbent dose, temperature, pH, and contact time. Different models of isotherm, kinetic, and thermodynamic were utilized andthe results indicate that the nature of heavy metals adsorption onto TRBW was homogeneous. According to the maximum adsorption capacities, the metals ranked as Pb> Cd> Zn> Cr> Ni, and adsorption capacities were 94.97, 73.85, 39.56, 38.34, and 36.33 mg/g, respectively.

Keywords: bentonite, heavy metal, isotherm, thermal remediation, hazardous waste.

INTRODUCTION

The industrial sector's development undoubtedly is significant, rapid, and has more advantages. However, it is not without drawbacks, where there are passive impacts on the environmental components due to solid and liquid waste. Industrial solid waste as bentonite waste produced from factories of recycling spent engine oil which is saturated with oil and discarded without efficient remediation, which characterized by mobility, and toxicity and has negative impacts on the environmental components, soil, and groundwater and directly on microbial population due to oil contains aromatic and aliphatic hydrocarbon (Jaber, 2020). Industrial liquid waste causes water pollution due to its tremendous heavy metals. The characteristics of heavy metals in aquatic environments are soluble, persistent, and non-degradable. Thus, living cells can absorb heavy metals easily (Ugwu et al., 2020).

The removal of heavy metals from the environment is very significant. Removal or recovery technologies of metal ions are filtration, ion exchange, chemical precipitation, chemical oxidation, electro-deposition, and membrane systems. These conventional methods are costly, energy-demanding, and often associated with discharging contaminated byproducts, hence utilizing the adsorption process due to the simplicity of equipment, operation, and a low-cost method of heavy metals removal from wastewater (Inglezakis et al., 2007; Güzel et al., 2015). Adsorption is a mechanism in which molecules or ions (called adsorbates) transport from a solution to adhere to a particle surface (called an adsorbent) through physical and chemical bonding.The adsorption capacity depends on the availability of active sites in the adsorbent particles and the accessibility of incoming molecules or ions to the active sites (Inglezakis et al., 2007). In recent decades, extensive efforts have been devoted to investigating

and characterizing new and low-cost adsorbents for specific heavy metals with high removal capacities. Moreover, several types of research utilized low-cost materials such as clay, agricultural waste, and industrial by-products as adsorbents for pollutant removal in an aqueous solution. The well-known types of agricultural waste that have been employed in the removal of heavy metals are maize stalks (Marin et al., 2021), palm date pits (Esmael et al., 2014), wasted black tea (Malakahmad et al., 2016), peanut shells, eucalyptus bark, nutshells, olive pips, plum seeds, pine sawdust, peach stones (Hansen et al., 2010), sesame seed cake powder, groundnut seed cake powder, and coconut cake powders (Pavan Kumar et al., 2019). Furthermore, industrial byproducts such as fired coal fly ash (Papandreou et al., 2007), red mud (Smičiklas et al., 2014), olive stone waste (Corral Bobadilla et al., 2020), blast furnace slag, sludge, dust (Ahmaruzzaman, 2011), waste rubber tire, waste slurry, lignin, fly ash, red mud (Hussain et al., 2021). Natural clay is a significant adsorbent for heavy metals and it is a low-cost material as well, environmentally friendly, and locally available material such as montmorillonite (de Pablo et al., 2011), smectite (Mbadcam et al., 2011), bentonite (Kaya and Ören, 2005), kaolinite [17, 18], vermiculite (Malandrino et al., 2006) and goethite (Abdus-Salam and Adekola, 2005).

Indeed, a broad range of natural adsorbent materials had used for treating a wide variety of pollutants. However, the ideal adsorbent should have specified properties for environmental and industrial applications. The objectives of this study are 1) thermally remediation of engine oil-contaminated bentonite waste and to diminish the negative impacts on the environmental

components, 2) identify the chemical and physical characteristics of TRBW using XRD, FTIR, SEM, EDS, and BET tests as a new adsorbent material, cheap, locally available, 3) examine the ability of (TRBW) to remove the heavy metals in the aqueous solution with different parameters such as initial concentration, adsorbent dose, contact time, pH, and temperature, and considered as an environmentally friendly method for heavy metals removal from aqueous solution, and 4) analysis of the experimental data with different models such as isotherms which included Langmuir, Freundlich, and Temkin, while the kinetics including (Pseudo-First-Order Kinetics, Pseudo-second-Order, intra-particle diffusion, and Elovich), and finally thermodynamic analysis.

MATERIALS AND METHODS

Preparation of the adsorbent

The plants of spent engine oil recycling [PSE-OR] use Bentonite clay as an adsorbent material for refining spent oil. The generated Bentonite waste (BW) or the industrial by-products were in massive quantities and saturated with oil; hence, it is combustible as shown in Figure 1a. The BW was remediated thermally in two phases, first, the self or direct combustion, where the energy source of this combustion is the residual oil, and the BW at this phase converts to black powder (Fig. 1b), Whilethe second phase, the black powder is burning in an electrical furnace at 700 °C for 100 minutes to achieve the desorption of residual oil and impurities (Cao et al., 2017; Kumar and Lingfa, 2020). In the later phase, it was reddish-white
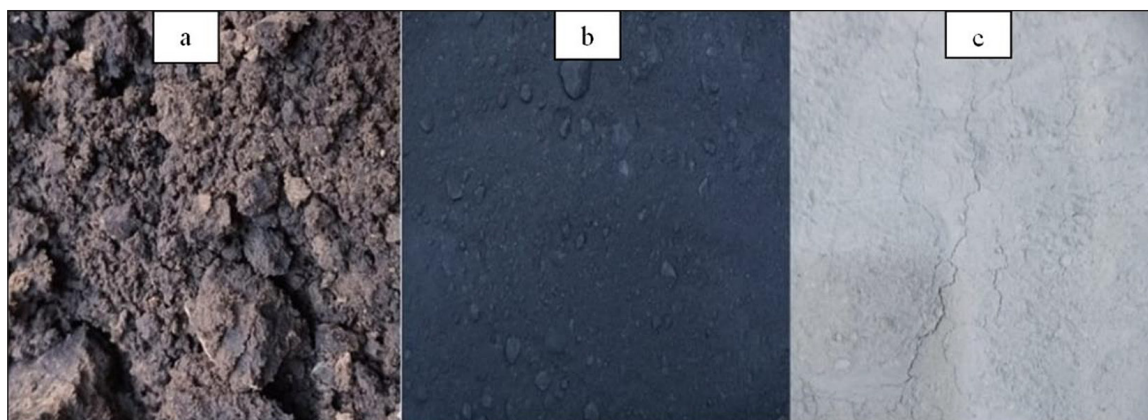
Figure 1. Bentonite clay: (a) contaminated bentonite waste, (b) bentonite waste after direct combustion, (c) bentonite waste after burning

powder (Fig. 1c). The Bentonite clay was composited from smectite with 69.1%, quartz 18.3%, zeolite 5.1%, plagioclase 4.7%, and feldspar 2% (Skvortsov et al., 2021).

Chemicals and apparatus

The chemicals used in this study were analytical grade, purchased from PanREAC. Co. (Spain), prepare stock solutions (1000 mg/L) by dissolving an appropriate amount of salts $ZnCl_2$, $NiCl_2.6H_2O$, $CdCl_2.H_2O$, $CrCl_3. 6H_2O$, and $PbCl_2$ in distilled water to prepare ions (Zn, Ni, Cd, Cr, and Pb) respectively, then, the stocks store in the refrigerator, and the demanded initial concentrations in the experiments prepare by diluting the stock solutions with different proportions of distilled water. The mountainous pH values of solutions were to the required value by adding the required amount of 0.4N HCl or NaOH in drops.

The heavy metal samples were investigated using the flame atomic absorption spectrophotometer (type: SHIMADZU, Model: AA-7000, JAPAN). The X-ray diffraction (XRD) of the RBW test was in the XRD using (XrdXpert PA analytical Phillips Holland) with a high-power CuKα radioactive basis (0.154 nm wavelength) created at 40 kV/40 mA. The scanning of samples with a step size of 0.02° and a counting time of 0.2 sec per step.

In a Fourier- transformed infrared (FTIR) spectroscopy test using FT-NIR Spectrometer (The Spectrum Two N; PerkinElmer., USA), the test range of the region was 4000–450 cm^{-1} at room temperature. The resolution scanning of the sample was 16 times at 4 cm^{-1}.

The RBW surface morphology has been scanned by high-resolution scanning electron microscopy (FESEM TESCN MIRA3 FRENCH). Energy Dispersive XRay Spectroscopy (EDX) analysis has been carried outto identify the total chemical compositions of the samples. BET test to identify the external, specific surface area, and pore size by the Brunauer Emmett Teller (BET) method using Micro-Active for TriStar II Plus 2.03, and also measure of N_2 adsorption-desorption isotherms for TRBW at -196.9 °C, where the sample weight of TRBW adsorbent was 116.9 mg for 6 hr.

Adsorption experiments

The experiments of adsorption were carried out with different parameters, pH (2–13), adsorbent dose of RBW (0.05, 0.1, 0.2, 0.5, 1, 2, and 3 g/100 ml), contact time (5, 10, 20, 40, 60, 100, and 150 min), temperature (30, 40, and 50 ċ) and initial metal concentration (10, 20, 50, 75, 100, 150, and 200 mg/L). At the adsorbent dose experiments, the parameters of initial concentration of 100 ppm, pH of 7, contact time of 30 min, and room temperature, where the optimum adsorbent dose was appointed equal to 0.2 g/100 mL. The equilibrium isotherm models were built from the results of initial concentration experiments. Moreover, the kinetic model and thermodynamic analysis were conducted based on the contact time and temperature experiments. The batch adsorption mode uses a graduated plastic beaker filled with 100 ml of (Cd, Cr, Pb, Ni, or Zn) solution. The agitation velocity for sample shaking was set at 300 rpm. The sample passed through filtration paper to attain the TRBW particles, then the concentration of metal ions was determined with the flame atomic absorption spectrophotometer. The removal efficiency % and the adsorption capacity (mg/g) of heavy metals were calculated using the following equations, respectively.

$$\text{Removal efficiency} \% = \left(\frac{C_i - C_e}{C_i}\right) * 100 \quad (1)$$

$$q_e = \frac{V(C_i - C_e)}{W} \quad (2)$$

where: C_i and C_e (mg/L) – the concentrations of the heavy metal in the initial and equilibrium times, respectively;
V (L) – the used volume of the solution in the test, and W (g) is the adsorbent weight.

RESULTS AND DISCUSSION

Characteristics of TRBW

Table 1 shows the structural parameters and elemental composition of TRBW obtained from BET and EDX tests, respectively. Figure 2 represents N2 adsorption-desorption isotherms linear where a high quantity was adsorbed near saturation pressure. The results of the EDX indicated that the essential elemental ranking of TRBW was O > Si > C > Al with a total percentage of more than 87% and less than 13 % for summation

of minor elements which ranked such as Mg > S > Ca > P and Na as shown in Figure 3.

Figures 4a and 4b show the FTIR spectroscopic analysis of TRBW before and after adsorption of different metals (Pb, Cd, Cr, Zn, and Ni) in the 400–4000 cm⁻¹ range, respectively. They verify the presence of functional groups that might be responsible for the adsorption process, variations in the peaks were apparent due to the adsorption of different metals by TRBW, where the absorbance bands of loaded adsorbents with Cr, Cd, and Pb are higher than with Ni, Zn, and free adsorbents, especially with bands of 1048 and 484 cm⁻¹. The broadband at the 3400 cm⁻¹ range was due to the stretching vibration of H-O-H of hydrogen-bonded inter-layer water molecules, (Cukrowicz et al., 2020; Ullah et al., 2021), and the weak absorbance band in the 2920 cm⁻¹ range appeared due to the stretching vibration of the C–H (Ewis et al., 2020; Huang et al., 2015),

another absorbance band at range 2360 was due to [-OH] stretching vibration (Mohammed et al., 2018). The 1652 cm⁻¹ band has belonged to the OH⁻ deformation of water (Fatiha & Belkacem, 2016; Ullah et al., 2021) or resulted from the H–OH bending vibration (Huang et al., 2015; Nwosu et al., 2018).

The band at 1404 cm⁻¹ is due to the carbonate's presence as impurities (Ma et al., 2016; Ritz et al., 2011). The high strong band (1050–1048) was associated with Si–O–Si Stretching vibrations which corresponds to the characteristic of the Bentonite clay group (Aguilar et al., 2020; Fatiha and Belkacem, 2016; Karapinar and Donat, 2009). The peaks at (794–789) wereas assigned to the Si–O stretching due to the presence of quartz (Fatiha and Belkacem, 2016), kaolin (Nwosu et al., 2018), and disordered tridymite (Paluszkiewicz et al., 2008). The weak peak was in the range of (678–668) and was an indicator

Table 1. Structural parameters of TRBW

Characteristics	Value	Elemental Composition	Weight %
Specific surface area (m²/g)	67.17	C	14.63
External surface area (m²/g)	77.29	O	32.34
Langmuir surface area, (m²/g)	994.94	Na	1.38
BET surface area (m²/g)	69.61	Mg	3.62
Total pore volume (cm³/g)	0.15	Al	9.09
Pore size, (nm)	8.54	Si	31.56
BJH adsorption cumulative surface area of pores (cm²/g)	116.72	P	1.8
BJH adsorption cumulative volume of pores (cm³/g)	0.23	S	3.38
BJH adsorption average pore diameter (nm)	7.80	Ca	2.2
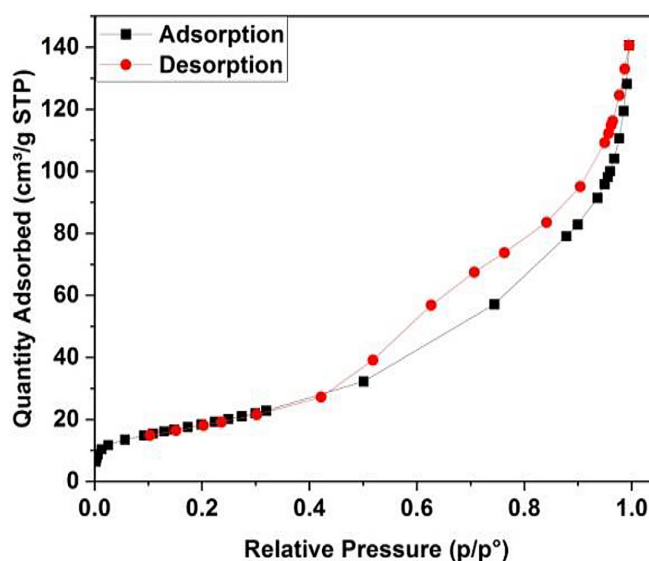
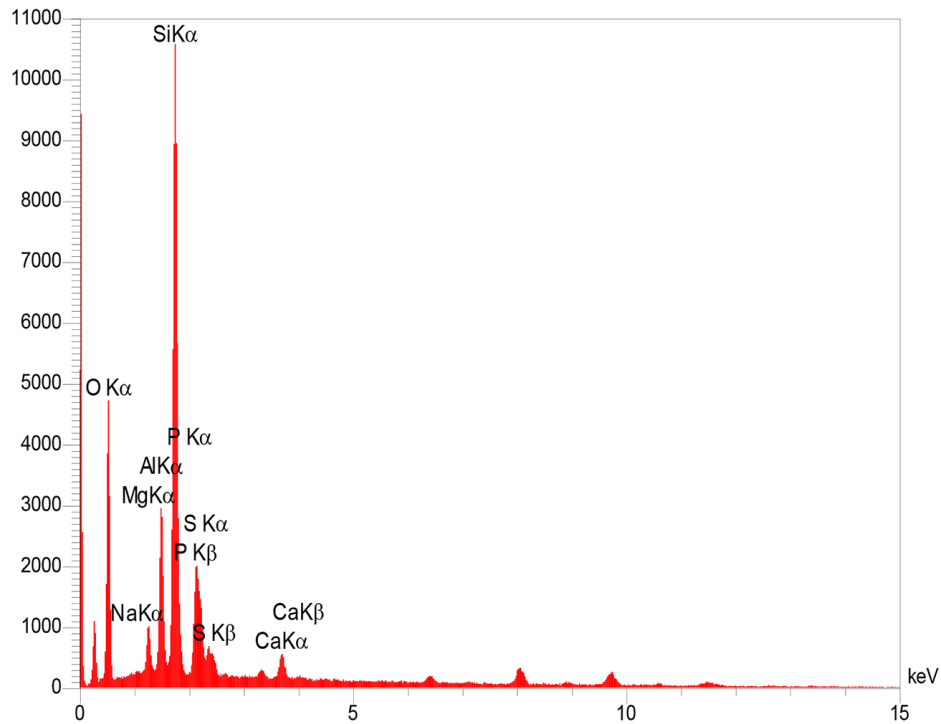**Figure 2.** Adsorption–desorption curves of TRBW
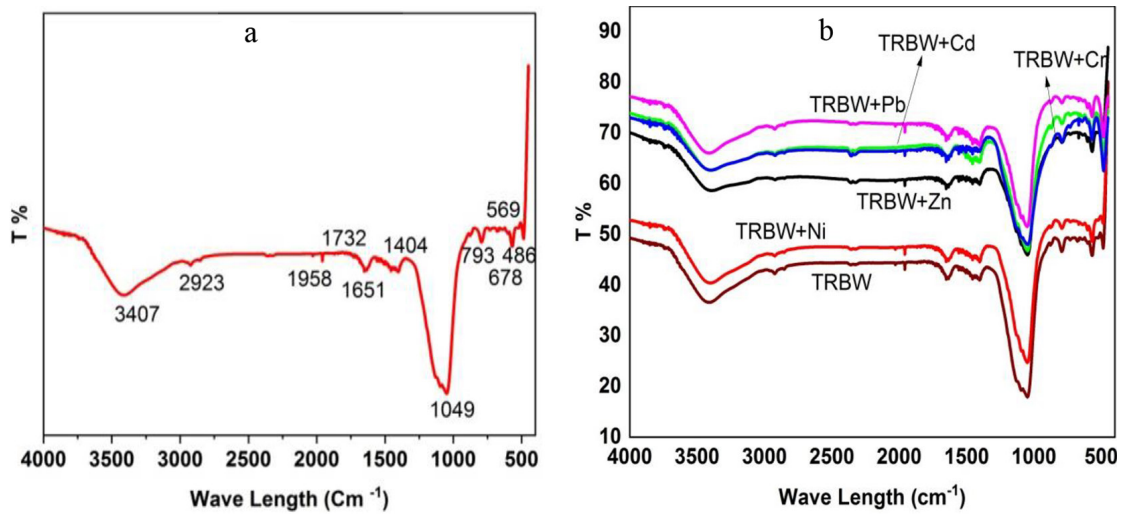
Figure 3. The EDS spectrum of TRBW

Figure 4. FTIR spectroscopic analysis of TRBW before adsorption (a) and after adsorption (b)

of the combined Al-O and Si-O bending vibration (Mohammed et al., 2018). The bands at 569 and 484 cm-1 were assigned to the deformation vibrations of Si–O–Al and Si–O–Si, respectively (Amari et al., 2018) or correspond to Si–O–Al and Si–O–Mg, respectively (Eloussaief et al., 2011).

Figure 5 shows SEM images that investigate the shape and surface morphology of the TRBW. The properties of the structure were layered and had small voids such as pores, cavities, and ravines. According to these properties, the opportunities for adsorption on the

Table 2. XRD Results of TRBW

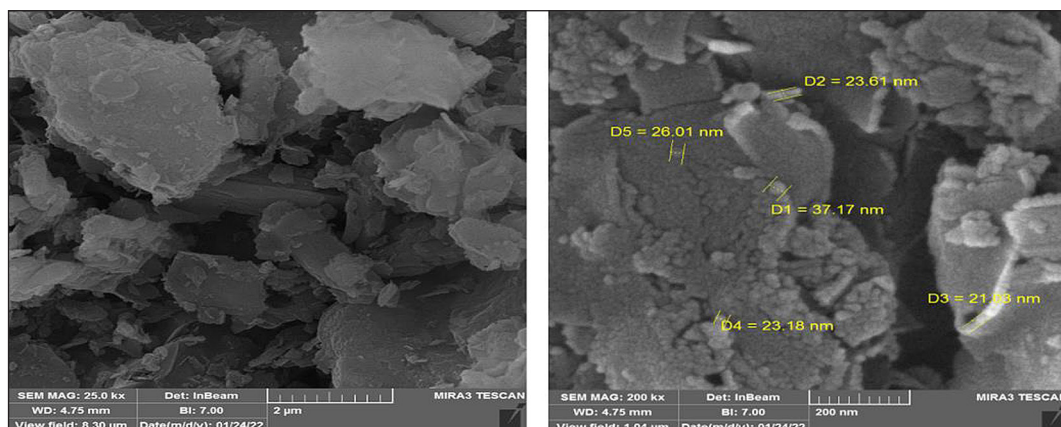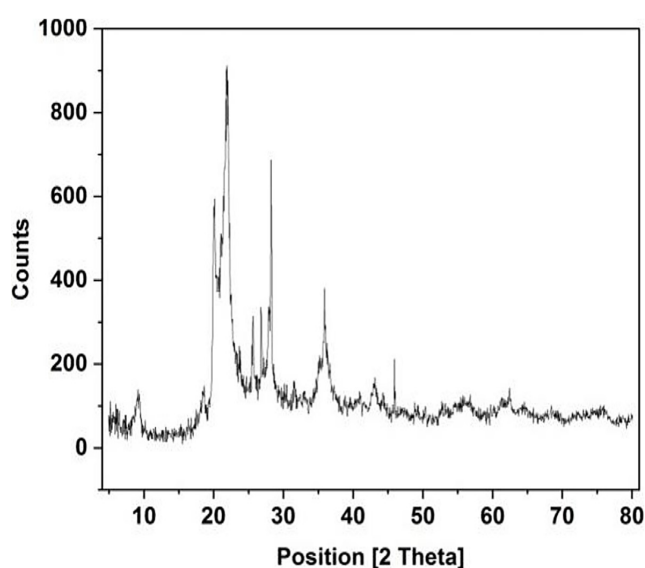| No.	Pos. [°2Th.]	FWHM [°2Th.]	d-spacing [A°]
1	9.26	0.590	9.550
2	18.54	0.492	4.785
3	19.98	0.246	4.444
4	21.96	0.394	4.047
5	25.66	0.197	3.472
6	26.81	0.148	3.326
7	28.24	0.148	3.160
8	35.93	0.197	2.499
9	43.07	0.787	2.100
10	45.97	0.18	1.973

Figure 5. SEM images of TRBW

Figure 6. The XRD patterns of TRBW

TRBW surface were high. Moreover, the presented voids assisted the metal ions in the deep penetration and binding to the active sites of TRBW, as reported in the literature (Mohammed et al., 2018). Also, according to the different colors and shapes, it is approved that the TRBW has more than one component. The XRD patterns analysis of TRBW showed Table 2 and Figure 6. The reflections at $2\theta = 9.26°$, 18.54°, 19.98°, 21.96°, 25.65°, 26.80°, 28.24°, 35.93°, 43.07°, and 45.97° can be observed for RBW. The peaks of 2θ (19.98°, 21.96°, and 35.93°) refer to the presence of montmorillonite, ($2\theta = 21.96°$, 25.66°, and 26.81°) to the quartz, ($2\theta = 43.07$ to calcite) and ($2\theta = 28.24°$ to the feldspar) as reported in the previous literature (Cukrowicz et al., 2020), (Taher et al., 2018), (Meneguin et al., 2017), (Chen et al., 2015) and (Đukić et al., 2015).

Factors affecting the heavy metals removal efficiency

Contact time

The experiments of contact time between heavy metals were carried out with varied periods in the range of 5–150 minutes with parameters of initial heavy metals concentration, the dose of TRBW, and the initial pH of the solution equaled to 100 ppm, 0.2 g/100 ml, and 6.5, respectively at room temperature. According to the adsorption removal efficiency shown in Figure 7a, it was apparent that the removal efficiency of heavy metals Pb, Cd, Zn, Cr, and Ni was affected by contact time where increasing contact time from (5 to 150 minutes) increase the removal efficiency from 95.8 to 98.0%, 83.1 to 93.4%, 58.4 to 80.3%, 58.5 to 70.6%, 55.6 to 66.9%) respectively. Moreover, the affinity of adsorbed heavy

metals to TRBW was different due to the electrochemical characterization of the self-metal ion (Shaheen et al., 2013). The ranking of adsorbed metal was listed where: Pb (II) > Cd (II) > Zn(II) > Cr(II) > Ni(II); therefore, it was apparent that TRBW had a superior activity for removal of heavy metals of (Pb, Cd) from aqueous solution with quick time. However, heavy metals (Zn, Cr, and Ni) had less transporting efficiency from the aqueous solution to the TRBW surface and required more time. The rapid adsorption at the start is due to the availability of a high number of binding zones on the adsorbent surface (Panda et al., 2020). It is apparent that the removal efficiency curves were less variation and more stability in the adsorption capacity occurring after the 30-minute; hence, the time of 30 minutes was utilized as a compromise time.

Initial pH

The nature of TRBW was alkaline due to the point zero charges (pH_{pzc}) of TRBW being 10.4; therefore, the pH of the aqueous solution shifts from neutral at the initial to 10.4 at the end of the experiment. The pH of the aqueous solution plays a significant role in the adsorption efficiency of metal ions onto clay surfaces (Đukić et al., 2015). The role of the pH values of aqueous solution in the removal of heavy metals was probed within the pH range 2–13 at ambient temperature utilizing 0.2 g/100 ml of TRBW dosage, adding 0.4 N of H_2SO_4 or NaOH solutions to adjust the pH of the aqueous solution.

The increases in removal efficiency were proportional to pH values, where an increase in the pH value from 2 to 13 increased the removal efficiency of Zn, Cr, and Ni from (57.2 to 99.4 %, 51.0 to 99.9%, and 54.9 to 99.9%, respectively. However, the maximum removal efficiency of Pb and Cd was (99.6% and 99.9%) at a pH value equal to 11 and lowered after (pH = 11) to equal 91.9% and 99.8%). Also, it was apparent that there was a marginal increase in the removal efficiency for Pb, and Cd with increasing pH value, as shown in Figure 7b.

Increasing the pH value increases the removal efficiency of heavy metals that result from elevating electrostatic forces of attraction due to the negative charges of the TRBW surface, leading to the adsorption of positively charged metal ions (Huang et al., 2015). Nonetheless, at a lower pH, the active sites of TRBW were more protonated, or in other meaning, At lower pH, the number of hydrogen ions is high then the metal ions have to compete between them for the accessing to active sites in TRBW, and consequently, the metal-ions are less accessible for binding with the active sites (Bhattacharyya & Gupta, 2006).

Temperature

The experiments of temperature effect on the removal efficiency were carried out at temperatures range of (30, 40, and 50 °C) where it was apparent that the increasing temperature leads to an increase in removal efficiency of heavy metals as shown in (Fig. 8a). The increase in removal efficiency was oblivious due to increasing temperature where remained concentrations in aqueous solution after the adsorption process for Pb, Cd, Zn, Cr, and Ni in 30 °C were (3.156, 11.571,
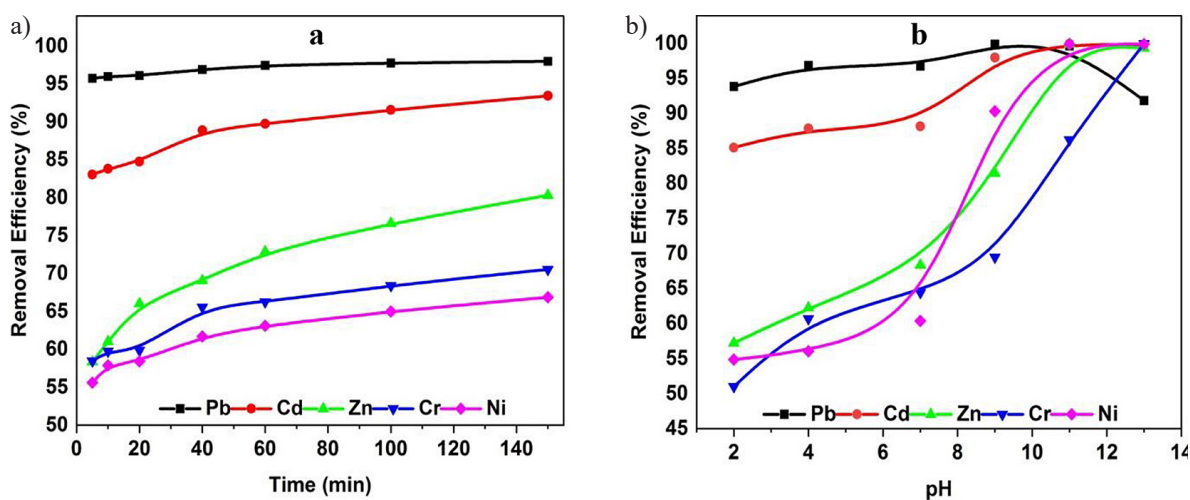
Figure 7. Effect of (a) contact timeand (b) pH on the heavy metals adsorption efficiency (concentration = 100 ppm, adsorbent dose = 0.2 g/100 ml, temperature of room)

31.868, 39.780, and 40.0355 ppm) while in 50 °C were (0.833, 3.012, 21.590, 31.471, and 32.779 ppm) respectively. Rising temperature reduces the viscosity of the aqueous solution and then increases the mobility and diffusion of the metal ions across the pores, the cavities, and the ravines of the adsorbent and then increases the adsorption capacity (Romdhane et al., 2020). So, the number of attracted metal ions to the active sites was high. Also, the benefit of temperature will be the extent of pore size and create new active sites on the adsorbent surface due to breaking the bonds (Gottipati, 2012).

Dose of adsorbent

The effect of TRBW dose on the removal efficiency was investigated using different ranges (0.05 to 3) g/100 ml of solution with constant parameters (initial concentration= 100 ppm, pH= 10.4, room temperature, agitation speed 300 rpm, and contact time 30 minutes). The removal efficiency of the metal ions with adsorbent doses was plotted in Figure 8b.

Increasing the dose of TRBW from (0.05 to 3) g/100 ml decreases the remained concentration of heavy metals (Pb, Cd, Zn, Cr, and Ni) in aqueous solution from 51.492 to 0.055 ppm, 63.915 to 0.2185 ppm, 78.9577 to 0.0884 ppm, 81.1654 to 0.1862 ppm, and 83.922 to 0.2310 ppm, where the removal efficiency increase from 48.51 to 99.95%, 36.09 to 99.78%, 21.04 to 99.91%, 18.84 to 99.81%, and 16.08 to 99.77%, respectively. Moreover, when the TRBW dose was equal to 0.5 g/100 mL, the removal efficiency of (Pb, Cd, Zn, Cr, and Ni) reached 98.8%, 97.9%, 99.2%, 96.5%, and 96.99%, respectively. Therefore, the finding exhibited that any increase of the dose above 0.5 g/100 ml of solution is not significant for metal ions removal due to the availability of active sites of RBW that prevents removing the entire metal ions (Mohammed et al., 2018). At low doses, the available active site is not adequate to absorb all metal ions in the
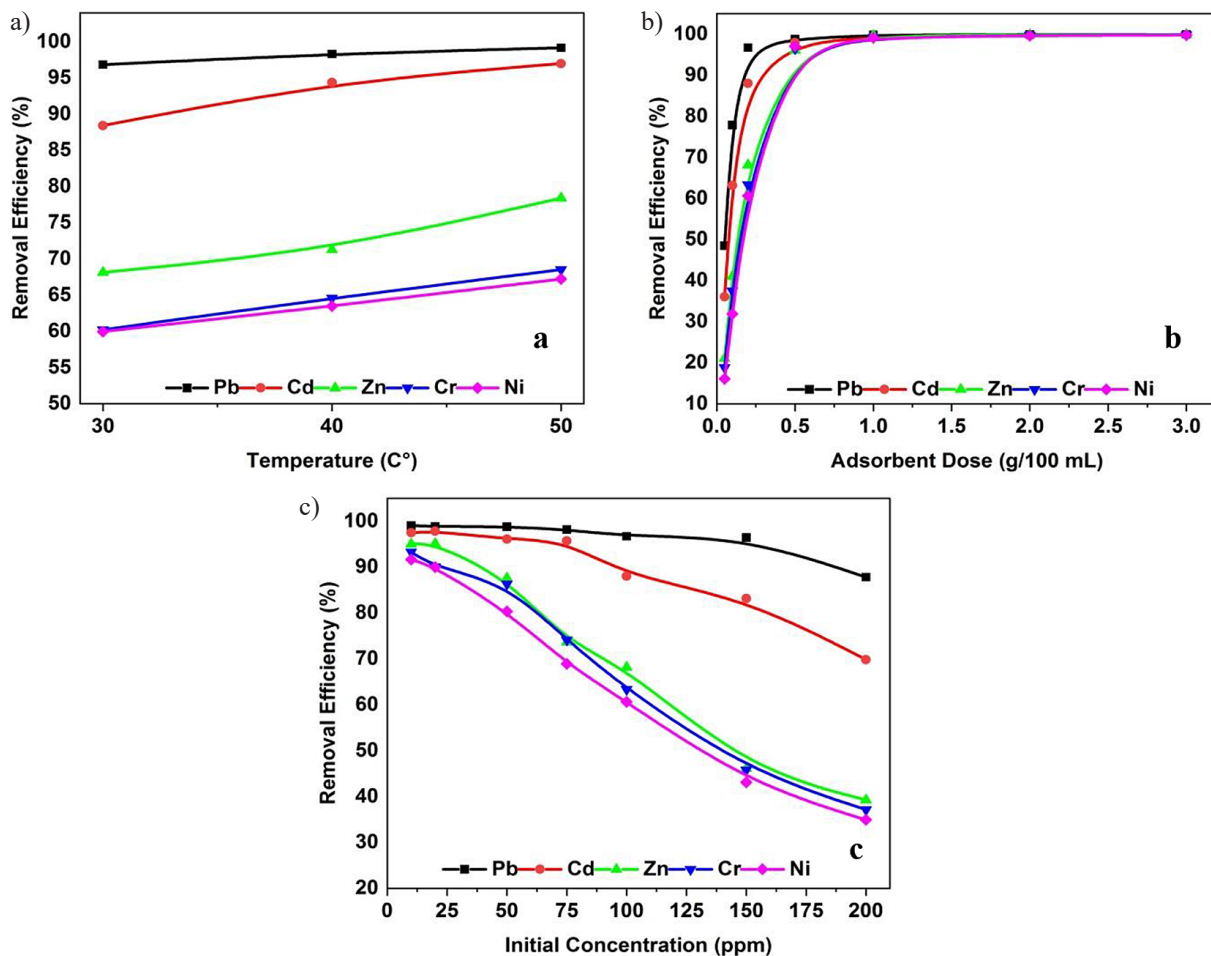
Figure 8. Effect of (a) temperature, (b) adsorbent dose, and (c) initial heavy metals concentration on removal efficiency (contact time = 30 minutes, pH = 10.4)

solution. The increase in adsorbent doses means more adsorption sites and surface area, consequently amounting to the quantity of metal ions removal (Potgieter et al., 2006).

Initial concentration of heavy metal

The effect of initial concentration of heavy metal was carried out with a varied range (10, 20, 50, 75, 100, 150 and 200) ppm with constant parameters (adsorbent dose = 0.2 gm/100 mL aqueous solution, agitation speed = 300 rpm, contact time 30 minutes, room temperature and pH = 10.4) as shown in Figure 8c, where an increase in the initial concentration of heavy metals (Pb, Cd, Zn, Cr, and Ni) from (10 to 200 ppm) decrease the removal efficiency from (99.1 to 87.9%, 97.5 to 69.9%, 95.0 to 39.2%, 93.3 to 37.1%, and 91.6 to 34.9%), respectively. High initial concentration accelerates the driving force and reduces the mass transfer resistance [48]. It was interpreted by the fact that at a fixed adsorbent dose, a fixed active site of the adsorbent was available for the adsorption of metal ions, and at elevated concentration, a greater interaction occurs by the metal ions remaining in the aqueous solution to be retained by the binding the active sites (Puchongkawarin et al., 2021).

Adsorption isotherm

The equilibrium adsorption or adsorption isotherm is designed to correlate the experimental data properly, where it results from relationship between adsorbate equilibrium concentration (C_e) per unit (mg) and quantity of the adsorbent per unit (g) at constant temperature, it is considered one of the most characteristics in the adsorption system to describe the interaction between the adsorbates and adsorbnet and also determine the optimum quantity of adsorbent. Isotherm parameters for the adsorption of metal ions on TRBW were estimated via linear and non-linear forms of the Langmuir (Eq. 3 and 4), Freundlich (Eq. 5 and 6), and Temkin (Eq. 7), respectively. The assumption of the Langmuir model depends on the reality that the adsorbate was adsorbed onto a monolayer adsorbent exterior with a limited number of homogeneous active sites on the adsorbent (Li et al., 2012).

$$\frac{C_e}{q_e} = \frac{1}{q_m * K_l} + \frac{C_e}{q_m} \qquad (3)$$

$$q_e = \frac{q_m}{1 + K_l * Ce} \qquad (4)$$

where: C_e (mg/L) and q_e (mg/g) – the remained concentration of metal ions and the number of metal ions adsorbed on unit adsorbents (TRBW in this study) in the solution after the equilibrium, respectively; K_l – the Langmuir constant representing the binding site's affinity; q_m (mg/g) – denotes the maximum adsorption capacity.

The separation factor *RL* is the fundamental characteristic that calculates from the Langmuir form (Belhadri et al., 2019):

$$RL = \frac{1}{1 + K_l * C_i} \qquad (5)$$

where: *RL* – indicates the type of isotherm to be irreversible (*RL* = 0), favorable (0 <*RL*< 1), linear (*RL* = 1) or unfavorable (RL > 1).

The Freundlich equation assumes the adsorption process is heterogeneous and onto a multilayer adsorbent surface (Li et al., 2012). (1/*n*) is the heterogeneity factor where the adsorbent surface is more heterogeneous if the value of (1/*n*) is close to zero, and it is favorable and promising if the *n* and K_f values are lying from (1 to 10) and from (1 to 20) respectively (Batool et al., 2018), (Belhadri et al., 2019).

This model is appropriate for the chemisorption (monolayer) and physisorption (multi-layer) systems (Freundlich, 1906).

$$log \, q_e = log K_f + \frac{1}{n} log C_e \qquad (6)$$

$$qe = K_f * C_e^{\left(\frac{1}{n}\right)} \qquad (7)$$

where: K_f ((mg/g) (L/mg)$^{1/n}$) – represents the adsorption capacity; 1/*n* – an indicator of the intensity of adsorption and depends on the heterogeneity of the material.

The third model of the molecules' adsorption onto heterogeneous externals is the Temkin model, which suggests that during the adsorption process, the adsorption heat leads to a linear decrease due to the interactions between the adsorbent and molecules (Mohammed et al., 2018).

$$q_e = B * \ln(K_t) + B * \ln(C_e) \qquad (8)$$

where: $B = RT/b$ – the constant of Temkin cor-
responding to the adsorption heat;
b (kJ/mol) – the heat of adsorption;
K_t (L/g) – the constant of equilibrium
binding that is related to the maximum
binding energy.

The parameters of models can be calculat-
ed from the slope and intercept that result from
the fitted plots. The average absolute deviation
(AAD%) was calculated using (Eq. 9), which also
was used for comparison between the isotherm
models in the prediction of adsorption capability
(Malakahmad et al., 2016).

$$AAD\ \% = 100 * \frac{\sum \sqrt{\frac{(Y_{actual} - Y_{model})^2}{Y_{actual}^2}}}{Number\ of\ Tests} \quad (9)$$

Tables 3 and 4 show the correlation coeffi-
cients (R^2), modeling and experimental adsorption
capacities, average absolute deviation (AAD%),
and constants of isotherm adsorption models in
linear and non-linear, respectively. The results of
all isotherms in linear and nonlinear have high
$R^2 > (0.9)$. However, the R^2 of linear Langmuir
was the highest and reached more than > 0.99.
The values of ADD% of linear isotherm were less
than nonlinear. Moreover, the results of ADD%
of the three linear isotherms were close to others.
A slight difference can be recognized between all
isotherms except the non-linear Freundlich has
high values of AAD.

According to Figure 9a and the data in Tables
3 and 4, the experimental maximum adsorp-
tion capacities (q_e) are close to the (q_m) obtained
from the Langmuir isotherm. Moreover, the lin-
ear Langmuir equation was better fitting than the

Table 3. Parameters of linear models of adsorption isotherm

Model	Parameters	Pb	Cd	Zn	Cr	Ni
				Linear		
Langmuir	q_m (mg/g)	94.97	73.85	39.56	38.34	36.33
	$q_{exp.}$ (mg/g)	87.83	69.86	39.25	37.13	34.95
	K_l (L/mg)	0.49	0.23	0.19	0.16	0.13
	R^2	0.996	0.993	0.994	0.998	0.998
	AAD %	9.06	14.89	18.07	7.19	8.29
Freundlich	K_f (L/mg)	24.14	13.89	8.49	7.09	6.37
	n	1.88	2.16	2.79	2.56	2.54
	R^2	0.926	0.920	0.918	0.913	0.934
	AAD %	8.22	7.57	7.65	7.06	6.66
Temkin	K_t (L/mg)	9.706	5.130	4.901	3.000	2.474
	B	15.93	12.02	6.16	6.47	6.22
	R^2	0.964	0.982	0.985	0.982	0.992
	AAD %	29.14	11.83	5.41	8.16	3.91

Table 4. Parameters of non-linear models of adsorption isotherm

| Model	Parameters	Pb	Cd	Zn	Cr	Ni
				Non-Linear		
Langmuir	q_m (mg/g)	95.37	70.27	37.66	37.38	35.58
	K_l (L/mg)	0.45	0.26	0.23	0.17	0.14
	R^2	0.974	0.96	0.967	0.993	0.991
	AAD %	10.95	11.52	10.19	5.71	6.65
Freundlich	K_f (L/mg)	31.54	19.52	11.86	10.67	9.38
	n	2.896	3.05	3.85	3.67	3.51
	R^2	0.9	0.936	0.91	0.893	0.917
	AAD %	45.25	34.85	25.48	28.42	23.61
Temkin	K_t (L/mg)	9.706	5.13	4.901	3.000	2.474
	B	15.925	12.021	6.165	6.465	6.216
	R^2	0.956	0.978	0.982	0.978	0.99
	AAD %	29.14	11.84	5.41	8.16	3.91
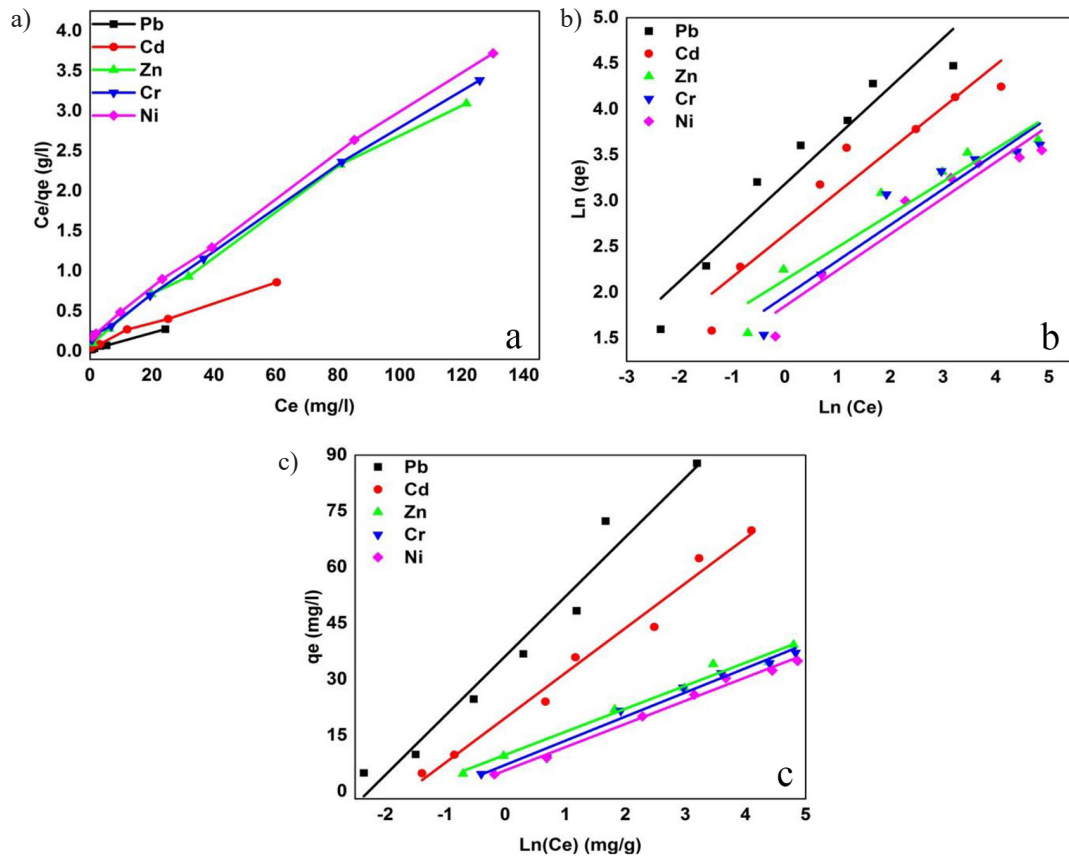
Figure 9. A plot of adsorption isotherms, (a) linear Langmuir isotherm, (b) linear Freundlich, and (c) linear Temkin
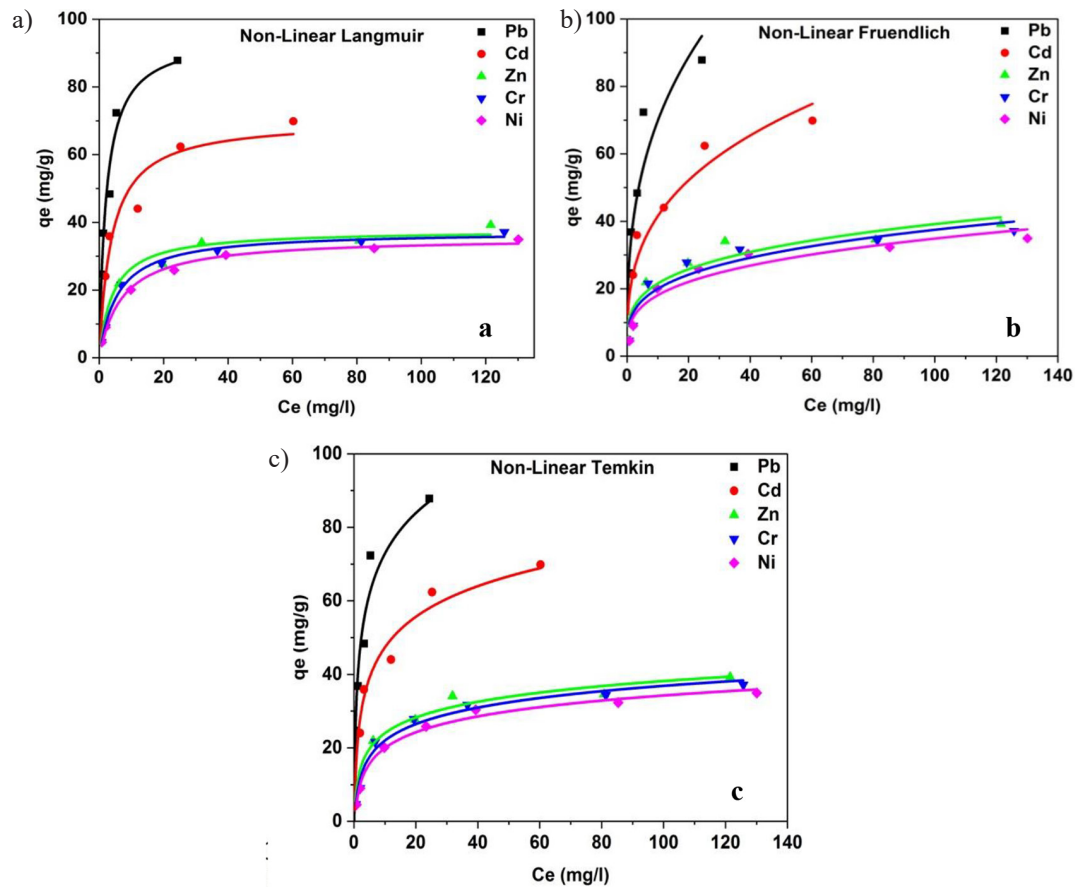

Figure 10. A plot of adsorption isotherms, (a) non-linear Langmuir, (b) Freundlich, and (c) Temkin isotherm

other isotherms according to high R^2 values. Also, the values of *RL* were arranged from (0.010 to 0.169), (0.021 to 0.300), (0.026 to 0.351), (0.031 to 0.393), and (0.0363 to 0.430) for Pb, Cd, Zn. Cr, and Ni, respectively, were an indicator that the adsorption was favorable. The n values of the Freundlich isotherm were more than (1) and smaller than (10), indicating that the adsorption of heavy metals onto TRBW is favorable, and the k_f values for linear and non-linear were arranged (1 to 20) except Pb more than 20 and this is indicator more heterogeneity. Moreover, the values of the correlation coefficient of Freundlich were good fitting and more than 0.9 as shown in Fig. 9b and 10b but less than Langmuir model. The results of the Temkin model were suitable where the values of correlation coefficient R^2 were more than 0.95 and good fitting as shown in Fig. 9c, and 10c, the binding constant was also high in addition to the values of B were more than 0, which was an indicator that the reactionary nature of the adsorption was exothermic due to the heat was released during the adsorption process.

Kinetics of adsorption

The study of adsorption kinetics is significant in describing the involved mechanisms of molecules' adsorption and the time necessary for the adsorption process (Batool et al., 2018). For the design of large sizes, adsorption facilities are very significant to study the mechanism of the adsorption process as a chemical reaction and mass transfer. An appropriate kinetic model is required to investigate the rate data (Riahi et al., 2017). Most of the kinetic models that were applied to fit the kinetic adsorption experiments are the pseudo-first-order (PFO), pseudo-second-order (PSO), Elovich, and intraparticle diffusion models (Simonin, 2016). The linear forms of kinetic models were employed to explain the transport of metal ions inside the adsorbent particles.

Pseudo-first-order kinetics

The pseudo-first-order (PFO) kinetics model is most suitable for the lowest concentrations of an aqueous solution. It was established by the relation of Lagergren based on the adsorbed amount. It is the first equation speed presented to explain the adsorption kinetics in a liquid/solid system. The following form is represented the linear model of pseudo-first-order (Miyah et al., 2017):

$$ln(q_e - q_t) = ln\, q_e - k_1 t \qquad (10)$$

where: qt (mg/g) and qe (mg/g) – the number of molecules adsorbed at a time (t) and equilibrium, respectively;
k_1 – the rate constant of adsorption of the (PFO) model (l·min^{-1}).
k_1 and $ln(qe)$ are equivalent to the slope and the interception of the straight line of the plot $ln\, (q_e - q_t)$ plot versus (t), respectively.

Pseudo-second order model [PSO]

The form of the PSO adsorption reaction model presented by (Ho et al., 1999) was obtained after the integration of equation 11 for the value of ($n = 2$) (Ho and McKay, 1999). It is appropriate for the small quantity of initial concentration (Ci) for the determination of initial adsorption capacity (q_e) (Batool et al., 2018).

$$\frac{dq_t}{dt} = k_n(q_e - q_t)^n \qquad (11)$$

It is assumed that the relationship between the adsorption capacity and the number of active sites occupied by the adsorbent is proportional. Besides linear equation 12, several other linearized equations have been presented in the interpretation of the experimental data.

$$\frac{t}{q_t} = \frac{1}{K_2 * q_e^2} + \frac{1}{q_e}(t) \qquad (12)$$

where: k_2 (g·mg^{-1}·min^{-1}) – the rate constant;
q_e (mg·g^{-1}) – the equilibrium adsorption capacity.

The values of q_e and k_2 were calculated from the slope and intercept of the straight line using the plot ln (t/q_t) plot versus (t), respectively.

Intra-particle diffusion equation

The ion exchange process consists of many steps, and to determine (rate-determining step) there is an urgent need for the intra-particle diffusion model due to this model is the most common method for identifying the rate-determining step (Ofomaja et al., 2020) using the following equation.

$$q_t = k_d t^{1/2} + c \qquad (13)$$

where: q_t – the number of molecules on the surface particle of the adsorbent at time t, (mg/g);
k_d – the intra-particle rate constant (mg/g·min$^{1/2}$);
t – the time (min);

c (mg/g) – a factor and is an indicator about the thickness of the boundary layer (Miyah et al., 2017).

The form of qt against $t^{1/2}$ should be linear. If the plot is not linear and does not pass through the origin point, this means that an intra-particle diffusion model could not be the only mechanism involved (Weber Jr & Morris, 1963).

The Elovich equation

Elovich's equation explains the kinetics of chemical adsorptions on heterogeneous surfaces of particlesdue to the interaction between the adsorbed ions that occurs during the adsorption process on the localized sites (Castro et al., 2018).

$$q_t = \left(\frac{1}{\beta}\right) ln(\alpha * \beta) + \frac{1}{\beta} ln t \qquad (14)$$

where: the parameter α (mg/g min) – the initial sorption rate;

β (g/mg) – the desorption constant related to the extent of the surface coverage and activation energy for the chemisorptions (Boulaiche et al., 2019).

The model which provides the higher value of R^2 and the lower value of standard deviation Δq is the more suitable model to represent the kinetic

adsorption. The following expression is the SD equation.

$$\Delta q \% = \sqrt{\frac{\Sigma \left[\frac{(q_{t,exp.} - q_{t,cal})}{q_{t,exp.}}\right]^2}{n-1}} * 100 \qquad (15)$$

Table 5 shows the correlation coefficients (R^2), standard deviation (Δq), experimental adsorption capacity (q_{exp}), and parameters of the above four equations where the results showed that the PFO model did not sufficiently fit the experimental values becausethe calculated equilibrium adsorption capacity $q_e$that results from the intercept value is smaller than the measured experimental q_t. The compatibility between the PFO model and experimental data is within a specified range of contact time and was generally suitable for the first 20–30 min of the adsorption process (Moussout et al., 2018); therefore, it presents confirmation that the heavy metal adsorption using TRBW did not obey the PFO model (Zulfikar et al., 2013). Figure 11a shows the behavior of heavy metals according to the PFO model.

From Table 5, the calculated equilibrium adsorption capacity (q_{cal}) using the linear PSO model was close to the experimental value (q_{exp}). Moreover, it has a high R^2 and low Δq values. Therefore, it can be provided as an indicator that PSO is

Table 5. Parameters of adsorption kinetic models

| Model	Parameter	Pb	Cd	Zn	Cr	Ni
Pseudo-first order	K_1 (min^{-1})	0.020	0.021	0.020	0.020	0.020
	q_{exp} (mg·g^{-1})	49.007	46.723	40.170	35.280	33.447
	q_{cal} (mg·g^{-1})	49.073	47.010	40.863	35.646	33.757
	R^2	0.993	0.972	0.972	0.971	0.975
	$\Delta q\%$	1.703	9.371	67.291	15.238	14.044
Pseudo-second order	K_2 (L·min^{-1})	0.063	0.012	0.005	0.010	0.011
	q_{exp} (mg·g^{-1})	49.007	46.723	40.170	35.280	33.105
	q_{cal} (mg·g^{-1})	49.075	46.408	39.507	34.918	33.117
	R^2	1.000	1.000	0.998	0.999	0.999
	$\Delta q\%$	1.610	1.000	12.273	9.825	9.036
Intra-particle diffusion	K_d (mg·g^{-1}·min$^{-1/2}$)	0.123	0.545	1.088	0.634	0.553
	C (mg·g^{-1})	47.625	40.358	27.424	27.883	26.970
	R^2	0.953	0.968	0.981	0.951	0.976
	$\Delta q\%$	0.205	0.824	1.669	1.644	1.054
Elovich	β (g·mg^{-1})	2.761	0.623	0.310	0.537	0.610
	α (mg·g^{-1}·min^{-1})	$1.3 \cdot 10^{56}$	$3.96 \cdot 10^{10}$	$4.53 \cdot 10^{2}$	$1.74 \cdot 10^{6}$	$6.67 \cdot 10^{6}$
	R^2	0.947	0.955	0.985	0.936	0.976
	$\Delta q\%$	0.947	1.011	1.669	1.986	1.081
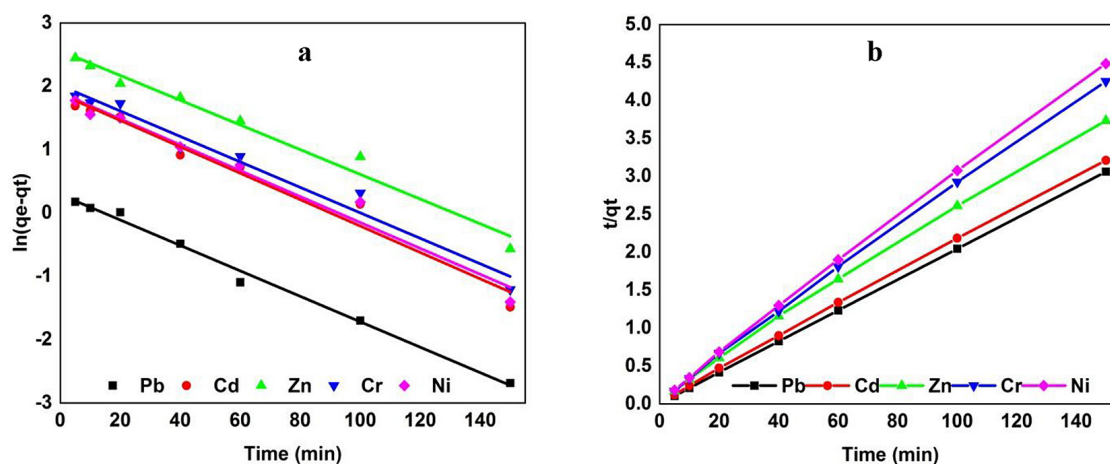
Figure 11. Kinetic study of heavy metals adsorption onto TRBW, (a) PFO model and PSO model (b)
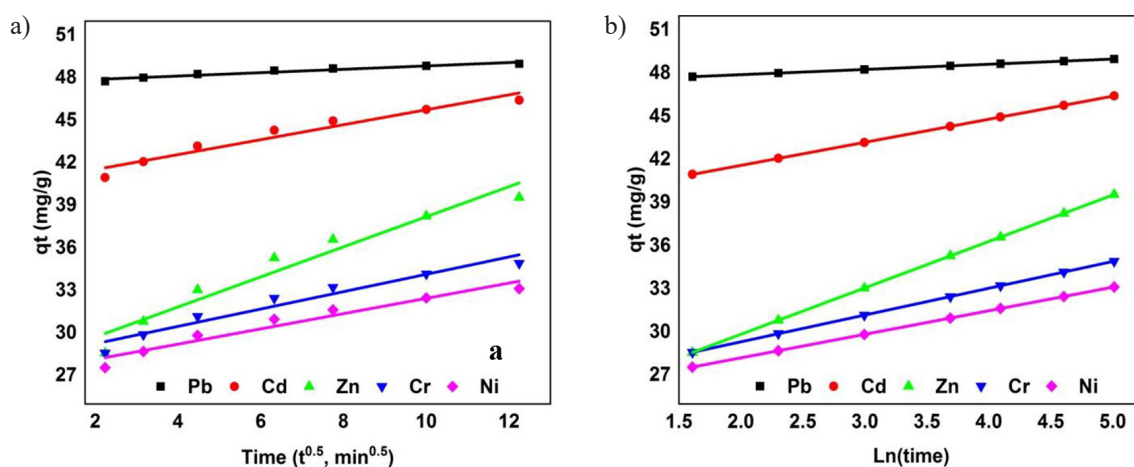

Figure 12. Kinetic study of heavy metals adsorption onto RBW, Intra-Particle Diffusion model (a) and Elovich model (b)

compatible with the adsorption process of heavy metals on the TRBW as shown in Figure 11b.

According to the high value of R^2, the Δq was the lowest; the experimental data is more compatible with the intra-particle diffusion model. Figure 12a explains that the plotting was in more than one region, and consequently, this indicates that the adsorption process resulted from more than one stage as external surface adsorption, intra-particle diffusion, and final equilibrium stage (Rostami et al., 2018).

The linear Elovich model was compatible with the experimental data by the correlation coefficient of R^2 and Δq value. However, the α value was very high.

Figure 12b shows the adsorption kinetics with the Elovich model. According to the R^2, Δq values, the experimental data are fitted to the intra-particle diffusion, pseudo-second-order, and the Elovich model, as previously reported in Table 6.

Adsorption thermodynamics analysis

It is significant to study the effect of temperature variation on adsorption. The constant of adsorption equilibrium K_c was determined from (Eq. 16) and is indispensable in the evaluation of the thermodynamic constants of the adsorbents (the change in enthalpy, $\Delta H°$, the change in entropy $\Delta S°$ and standard free Gibbs energy, $\Delta G°$).

$$K_c = \frac{q_e}{Ce} \qquad (16)$$

where: C_e and q_e– the equilibrium concentration and equilibrium adsorption respectively.

$$\ln K_c = \frac{-\Delta H°}{RT} + \frac{\Delta S°}{R} \qquad (17)$$

where: $\Delta H°$ and $\Delta S°$ – for the adsorption process are calculated from a slope and an intercept that result from Eq. 17 (Van't Hoff Equation).

Table 6. Parameters of adsorption thermodynamic analysis

Ions	$\Delta H°$ (KJ/mol)	$\Delta S°$ (KJ/mol K)	$\Delta G°$ (KJ/mol)			R^2
			30 K	40 K	50 K	
Pb	54.87	203.64	-6.88	-8.78	-10.96	0.999
Cd	58.55	204.52	-3.38	-5.54	-7.46	0.999
Zn	21.55	71.65	-0.17	-0.87	-1.60	0.999
Cr	14.77	46.35	0.70	0.31	-0.23	0.999
Ni	11.09	34.57	0.62	0.25	-0.07	0.999

Table 7. Comparison with previous study of the maximum adsorption capacity of heavy metals

Adsorbent	Adsorbate	q_m (mg/g)	Reference
Bentonite coated with Fe_3O_4 magnetite nanoparticles	Zn(II)	22.6	(Mohammed et al., 2018)
Active carbon	Pb(II) Zn(II)	6.7 11.2	(Mishra & Patel, 2009)
Bentonite	Pb(II) Zn(II)	7.6 9.1	
Barbadensis Miller waste leaves powder	Ni(II)	10	(Gupta & Kumar, 2019)
Lignite	Cd(II)	38	(Jellali et al., 2021)
Esterified spent grain	Cd(II)	473.9	(Li et al., 2012)
Natural bentonite	Zn(II)	68.5	(Sen & Gomez, 2011)
Acid modified montmorillonite	Zn(II) Cd(II) Pb(II) Ni(II)	76.92 0.62 1.62 4.00	(Akpomie & Dawodu, 2016)
Organo-bentonite	Cr(VI)	10.04	(Castro-Castro et al., 2020)
Thermal remediated bentonite waste (TRBW)	Pb (II)	94.97	This study
	Cd (II)	73.85	
	Zn (II)	39.56	
	Cr (II)	38.34	
	Ni (II)	36.33	

The endothermic, reversibility, and spontaneity of the process were determined based on the change in enthalpy ($\Delta H°$), the entropy ($\Delta S°$), and the Gibbs energy ($\Delta G°$), respectively. From the results in Table 6, it showed that the adsorption process was spontaneous and endothermic due to the negative ($\Delta G°$) and positive ($\Delta H°$) respectively, and the positive ($\Delta S°$) is an indicator of the randomness at the interface of solid-solution during adsorption (Boulaiche et al., 2019; Kim & Kim, 2019).

Comparison of adsorption capacity

Using industrial solid waste as an adsorbent for the removal of heavy metals should possess several specifications, effective for the adsorption of a broad number of heavy metals, low cost, easily disposed of after adsorption or regeneration, and environment-friendly utilization. Table 7 summarizes the previous studies for comparison according to the adsorption capacity.

CONCLUSIONS

Thermal remediation of bentonite waste results from factories recycling spent engine oil to minimize the risks to the environment and living beings by destroying all adhered hydrocarbon components. The color of obtained TRBW is a reddish-white powder with specific surface area, pore volume, and pore size equaled 67.17 m²/g, 0.15 cm³/g, and 8.54 nm, respectively. From the experimental data and the results of the analysis can be concluded that the ability of using TRBW as anovel and a low-cost adsorbent for heavy metals removal in an aqueous solution.

The TRBW can be employed in the practical application of industrial wastewater treatment by batch and dynamic flow methods with a wide range of parameters, initial concentration, contact time, temperature, and pH that have a role in the adsorption capacity. The XRD patterns, FTIR analysis, SEM images, BET, and EDS spectra

areas indicators of the capability of TRBW for adsorption of the pollutants in an aqueous solution due to the chemical and morphological structure.

Due to the mineral, chemical structure, and alkalinity nature of TRBW, which create appropriate conditions for heavy metals adsorption where the maximum adsorptions of Pb, Cd, Zn, Cr, and Ni are 94.97, 73.85, 39.56, 38.34 and 36.33 mg/g, respectively. By using three models inisotherm analysis, langmuir, freundlich, and temkin, it showed that the experimental data were more fitted to the langmuir model, and according to these results, it indicated that adsorption of the heavy metals onto the TRBWwas homogeneous, and from values of n and k_l, the adsorption phenomena were favorable.

REFERENCES

1. Abdus-Salam, N.,Adekola, F.A. 2005. The influence of pH and adsorbent concentration on adsorption of lead and zinc on a natural goethite. African Journal of Science and Technology, 6(2).

2. Aguilar, J., Almeida-Naranjo, C., Aldás, M. B., Guerrero, V.H. 2020. Acid activation of bentonite clay for recycled automotive oil purification. E3S Web of Conferences, 191, 03002.

3. Ahmaruzzaman, M. 2011. Industrial wastes as low-cost potential adsorbents for the treatment of wastewater laden with heavy metals. Advances in Colloid and Interface Science, 166(1–2), 36–59.

4. Akpomie, K.G., Dawodu, F.A. 2016. Acid-modified montmorillonite for sorption of heavy metals from automobile effluent. Beni-Suef University Journal of Basic and Applied Sciences, 5(1), 1–12.

5. Al-Essa, K., Khalili, F. 2018. Heavy metals adsorption from aqueous solutions onto unmodified and modified Jordanian kaolinite clay: Batch and column techniques. American Journal of Applied Chemistry, 6(1), 25–34.

6. Amari, A., Gannouni, H., Khan, M.I., Almesfer, M.K., Elkhaleefa, A.M., Gannouni, A. 2018. Effect of structure and chemical activation on the adsorption properties of green clay minerals for the removal of cationic dye. Applied Sciences, 8(11), 2302.

7. Batool, F., Akbar, J., Iqbal, S., Noreen, S., Bukhari, S.N.A. 2018. Study of isothermal, kinetic, and thermodynamic parameters for adsorption of cadmium: An overview of linear and nonlinear approach and error analysis. Bioinorganic Chemistry and Applications, 2018.

8. Belhadri, M., Mokhtar, A., Meziani, S., Belkhadem, F., Sassi, M., Bengueddach, A. 2019. Novel low-cost adsorbent based on economically modified bentonite for lead (II) removal from aqueous solutions. Arabian Journal of Geosciences, 12(3), 1–13.

9. Bhattacharyya, K.G., Gupta, S.S. 2006. Kaolinite, montmorillonite, and their modified derivatives as adsorbents for removal of Cu (II) from aqueous solution. Separation and Purification Technology, 50(3), 388–397.

10. Boulaiche, W., Hamdi, B., Trari, M. 2019. Removal of heavy metals by chitin: Equilibrium, kinetic and thermodynamic studies. Applied Water Science, 9(2), 1–10.

11. Cao, C.-Y., Liang, C.-H., Yin, Y., Du, L.-Y. 2017. Thermal activation of serpentine for adsorption of cadmium. Journal of Hazardous Materials, 329, 222–229.

12. Castro, L., Blázquez, M.L., González, F., Muñoz, J.A., Ballester, A. 2018. Heavy metal adsorption using biogenic iron compounds. Hydrometallurgy, 179, 44–51.

13. Castro-Castro, J.D., Macías-Quiroga, I.F., Giraldo-Gomez, G.I., Sanabria-González, N.R. 2020. Adsorption of Cr (VI) in aqueous solution using a surfactant-modified bentonite. The Scientific World Journal, 2020.

14. Chen, C., Liu, H., Chen, T., Chen, D., Frost, R.L. 2015. An insight into the removal of Pb (II), Cu (II), Co (II), Cd (II), Zn (II), Ag (I), Hg (I), Cr (VI) by Na (I)-montmorillonite and Ca (II)-montmorillonite. Applied Clay Science, 118, 239–247.

15. Corral Bobadilla, M., Lostado Lorza, R., Somovilla Gómez, F., Escribano García, R. 2020. Adsorptive of nickel in wastewater by olive stone waste: Optimization through multi-response surface methodology using desirability functions. Water, 12(5), 1320.

16. Cukrowicz, S., Grabowski, B., Kaczmarska, K., Bobrowski, A., Sitarz, M., Tyliszczak, B. 2020. Structural Studies (FTIR, XRD) of Sodium Carboxymethyl Cellulose Modified Bentonite. Archives of Foundry Engineering, 20.

17. de Pablo, L., Chávez, M.L., Abatal, M. 2011. Adsorption of heavy metals in acid to alkaline environments by montmorillonite and Ca-montmorillonite. Chemical Engineering Journal, 171(3), 1276–1286.

18. Đukić, A.B., Kumrić, K.R., Vukelić, N.S., Dimitrijević, M.S., Baščarević, Z.D., Kurko, S.V., Matović, L.L. 2015. Simultaneous removal of Pb^{2+}, Cu^{2+}, Zn^{2+} and Cd^{2+} from highly acidic solutions using mechano-chemically synthesized montmorillonite–kaolinite/TiO_2 composite. Applied Clay Science, 103, 20–27.

19. Eloussaief, M., Kallel, N., Yaacoubi, A., Benzina, M. 2011. Mineralogical identification, spectroscopic characterization, and potential environmental use of natural clay materials on chromate removal from aqueous solutions. Chemical Engineering Journal, 168(3), 1024–1031.

20. Esmael, A.I., Matta, M.E., Halim, H.A., Azziz, F.A. 2014. Adsorption of heavy metals from industrial wastewater using palm date pits as low cost adsorbent. Int J Eng Adv Technol, 3, 71–76.

21. Ewis, D., Benamor, A., Ba-Abbad, M.M., Nasser, M., El-Naas, M., Qiblawey, H. 2020. Removal of oil content from oil-water emulsions using iron oxide/ bentonite nano adsorbents. Journal of Water Process Engineering, 38, 101583.

22. Fatiha, M., Belkacem, B. 2016. Adsorption of methylene blue from aqueous solutions using natural clay. J. Mater. Environ. Sci, 7(1), 285–292.

23. Gottipati, R. 2012. Preparation and characterization of microporous activated carbon from biomass and its application in the removal of chromium (VI) from aqueous phase.

24. Gupta, S., Kumar, A. 2019. Removal of nickel (II) from aqueous solution by biosorption on A. barbadensis Miller waste leaves powder. Applied Water Science, 9(4), 1–11.

25. Güzel, F., Sayğılı, H., Sayğılı, G.A., Koyuncu, F. 2015. New low-cost nanoporous carbonaceous adsorbent developed from carob (Ceratonia siliqua) processing industry waste for the adsorption of anionic textile dye: Characterization, equilibrium and kinetic modeling. Journal of Molecular Liquids, 206, 244–255.

26. Hansen, H.K., Arancibia, F., Gutiérrez, C. 2010. Adsorption of copper onto agriculture waste materials. Journal of Hazardous Materials, 180(1–3), 442–448.

27. Ho, Y.-S., McKay, G. 1999. Pseudo-second order model for sorption processes. Process Biochemistry, 34(5), 451–465.

28. Huang, L., Zhou, Y., Guo, X., Chen, Z. 2015. Simultaneous removal of 2, 4-dichlorophenol and Pb (II) from aqueous solution using organoclays: Isotherm, kinetics and mechanism. Journal of Industrial and Engineering Chemistry, 22, 280–287.

29. Hussain, S., Abid, M.A., Munawar, K.S., Saddiqa, A., Iqbal, M., Suleman, M., Hussain, M., Riaz, M., Ahmad, T., Abbas, A. 2021. Choice of suitable economic adsorbents for the reduction of heavy metal pollution load. Polish Journal of Environmental Studies, 30(3).

30. Inglezakis, V.J., Stylianou, M.A., Gkantzou, D., Loizidou, M.D. 2007. Removal of Pb (II) from aqueous solutions by using clinoptilolite and bentonite as adsorbents. Desalination, 210(1–3), 248–256.

31. Jaber, W. 2020. Sorption of engine oil from aqueous solution into ricinus communis leaves in three-phase fluidized bed reactor [Thesis]. Baghdad.

32. Jalees, M.I., Farooq, M.U., Basheer, S., Asghar, S. 2019. Removal of heavy metals from drinking water using Chikni Mitti (kaolinite): Isotherm and kinetics. Arabian Journal for Science and Engineering, 44(7), 6351–6359.

33. Jellali, S., Azzaz, A.A., Jeguirim, M., Hamdi, H., Mlayah, A. 2021. Use of lignite as a low-cost material for cadmium and copper removal from aqueous solutions: Assessment of adsorption characteristics and exploration of involved mechanisms. Water, 13(2), 164.

34. Karapinar, N., Donat, R. 2009. Adsorption behaviour of Cu2+ and Cd2+ onto natural bentonite. Desalination, 249(1), 123–129.

35. Kaya, A., Ören, A.H. 2005. Adsorption of zinc from aqueous solutions to bentonite. Journal of Hazardous Materials, 125(1–3), 183–189.

36. Kim, Y.-S., Kim, J.-H. 2019. Isotherm, kinetic and thermodynamic studies on the adsorption of paclitaxel onto Sylopute. The Journal of Chemical Thermodynamics, 130, 104–113.

37. Kumar, A., Lingfa, P. 2020. Sodium bentonite and kaolin clays: Comparative study on their FT-IR, XRF, and XRD. Materials Today: Proceedings, 22, 737–742.

38. Li, Q., Chai, L., & Qin, W. (2012). Cadmium (II) adsorption on esterified spent grain: Equilibrium modeling and possible mechanisms. Chemical Engineering Journal, 197, 173–180.

39. Ma, L., Chen, Q., Zhu, J., Xi, Y., He, H., Zhu, R., Tao, Q., Ayoko, G.A. 2016. Adsorption of phenol and Cu (II) onto cationic and zwitterionic surfactant modified montmorillonite in single and binary systems. Chemical Engineering Journal, 283, 880–888.

40. Malakahmad, A., Tan, S., Yavari, S. 2016. Valorization of wasted black tea as a low-cost adsorbent for nickel and zinc removal from aqueous solution. Journal of Chemistry, 2016.

41. Malandrino, M., Abollino, O., Giacomino, A., Aceto, M., Mentasti, E. 2006. Adsorption of heavy metals on vermiculite: Influence of pH and organic ligands. Journal of Colloid and Interface Science, 299(2), 537–546.

42. Marin, N.M., Dinu, L., Stanculescu, I., Cristea, N.I., Ionescu, A.I. 2021. Maize stalk material for on-site treatment of highly polluted leachate and mine wastewater. Materials, 14(4), 956.

43. Mbadcam, J.K., Anagho, S.G., Nsami, J.N. 2011. Kinetic and equilibrium studies of the adsorption of lead (II) ions from aqueous solution onto two Cameroon clays: Kaolinite and smectite. Journal of Environmental Chemistry and Ecotoxicology, 3(11), 290–297.

44. Meneguin, J.G., Moisés, M.P., Karchiyappan, T., Faria, S.H.B., Gimenes, M.L., de Barros, M.A.S., Venkatachalam, S. 2017. Preparation and characterization of calcium treated bentonite clay and its application for the removal of lead and cadmium ions: Adsorption and thermodynamic modeling. Process Safety and Environmental Protection, 111, 244–252.

45. Mishra, P.C., Patel, R.K. 2009. Removal of lead and zinc ions from water by low cost adsorbents. Journal of Hazardous Materials, 168(1), 319–325.

46. Miyah, Y., Lahrichi, A., Idrissi, M., Boujraf, S., Taouda, H., Zerrouq, F. 2017. Assessment of adsorption kinetics for removal potential of Crystal Violet dye from aqueous solutions using Moroccan pyrophyllite. Journal of the Association of Arab Universities for

Basic and Applied Sciences, 23, 20–28.

47. Mohammed, A.A., Brouers, F., Sadi, S.I., Al-Musawi, T.J. 2018. Role of Fe3O4 magnetite nanoparticles used to coat bentonite in zinc (II) ions sequestration. Environmental Nanotechnology, Monitoring & Management, 10, 17–27.

48. Moussout, H., Ahlafi, H., Aazza, M., Maghat, H. 2018. Critical of linear and nonlinear equations of pseudo-first order and pseudo-second order kinetic models. Karbala International Journal of Modern Science, 4(2), 244–254.

49. Nwosu, F.O., Ajala, O.J., Owoyemi, R.M., Raheem, B.G. 2018. Preparation and characterization of adsorbents derived from bentonite and kaolin clays. Applied Water Science, 8(7), 1–10.

50. Ofomaja, A.E., Naidoo, E.B., Pholosi, A. 2020. Intraparticle diffusion of Cr (VI) through biomass and magnetite coated biomass: A comparative kinetic and diffusion study. South African Journal of Chemical Engineering, 32(1), 39–55.

51. Paluszkiewicz, C., Holtzer, M., Bobrowski, A. 2008. FTIR analysis of bentonite in moulding sands. Journal of Molecular Structure, 880(1–3), 109–114.

52. Panda, L., Jena, S.K., Rath, S.S., Misra, P.K. 2020. Heavy metal removal from water by adsorption using a low-cost geopolymer. Environmental Science and Pollution Research, 27(19), 24284–24298.

53. Papandreou, A., Stournaras, C.J., Panias, D. 2007. Copper and cadmium adsorption on pellets made from fired coal fly ash. Journal of Hazardous Materials, 148(3), 538–547.

54. Pavan Kumar, G., Malla, K.A., Yerra, B., Srinivasa Rao, K. 2019. Removal of Cu (II) using three low-cost adsorbents and prediction of adsorption using artificial neural networks. Applied Water Science, 9(3), 1–9.

55. Potgieter, J.H., Potgieter-Vermaak, S.S., Kalibantonga, P.D. 2006. Heavy metals removal from solution by palygorskite clay. Minerals Engineering, 19(5), 463–470.

56. Puchongkawarin, C., Mattaraj, S., Umpuch, C. 2021. Experimental and modeling studies of methylene blue adsorption onto Na-Bentonite clay. Engineering and Applied Science Research, 48(3), 268–279.

57. Riahi, K., Chaabane, S., Thayer, B.B. 2017. A kinetic modeling study of phosphate adsorption onto Phoenix dactylifera L. date palm fibers in batch mode. Journal of Saudi Chemical Society, 21, S143–S152.

58. Ritz, M., Vaculíková, L., Plevová, E. 2011. Application of infrared spectroscopy and chemometric methods to identification of selected minerals.

59. Romdhane, D.F., Satlaoui, Y., Nasraoui, R., Charef, A., Azouzi, R. 2020. Adsorption, modeling, thermodynamic, and kinetic studies of methyl red removal from textile-polluted water using natural and purified organic matter rich clays as low-cost adsorbent. Journal of Chemistry, 2020.

60. Rostami, E., Norouzbeigi, R., Rahbar, A. 2018. Thermal and chemical modification of bentonite for adsorption of an anionic dye. Advances in Environmental Technology, 4(1), 1–12.

61. Sen, T.K., Gomez, D. 2011. Adsorption of zinc (Zn^{2+}) from aqueous solution on natural bentonite. Desalination, 267(2–3), 286–294.

62. Shaheen, S.M., Tsadilas, C.D., Rinklebe, J. 2013. A review of the distribution coefficients of trace elements in soils: Influence of sorption system, element characteristics, and soil colloidal properties. Advances in Colloid and Interface Science, 201, 43–56.

63. Shirsath, D.S., Shirivastava, V.S. 2015. Adsorptive removal of heavy metals by magnetic nanoadsorbent: An equilibrium and thermodynamic study. Applied Nanoscience, 5(8), 927–935.

64. Simonin, J.-P. 2016. On the comparison of pseudo-first order and pseudo-second order rate laws in the modeling of adsorption kinetics. Chemical Engineering Journal, 300, 254–263.

65. Skvortsov, A.V., Islamova, G.G., Ryazanova, A.S., Sayakhov, R.I., Mishagin, K.A., Tverdov, I.D., Khayrullina, Z.Z., Khatsrinova, Y.A. 2021. Development of organobentonite based on bentonite clay for the purpose of disposing of oil spills on water bodies. IOP Conference Series: Earth and Environmental Science, 815(1), 012036.

66. Smičiklas, I., Smiljanić, S., Perić-Grujić, A., Šljivić-Ivanović, M., Mitrić, M., Antonović, D. 2014. Effect of acid treatment on red mud properties with implications on Ni (II) sorption and stability. Chemical Engineering Journal, 242, 27–35.

67. Taher, T., Rohendi, D., Mohadi, R., Lesbani, A. 2018. Thermal and Acid Activation (TAA) of bentonite as adsorbent for removal of methylene blue: A kinetics and thermodynamic study. Chiang Mai Journal of Science, 45(4), 1770–1781.

68. Ugwu, E.I., Tursunov, O., Kodirov, D., Shaker, L.M., Al-Amiery, A.A., Yangibaeva, I., Shavkarov, F. 2020. Adsorption mechanisms for heavy metal removal using low cost adsorbents: A review. IOP Conference Series: Earth and Environmental Science, 614(1), 012166.

69. Ullah, S., Ur Rahman, A., Ullah, F., Rashid, A., Arshad, T., Viglašová, E., Galamboš, M., Mahmoodi, N.M., Ullah, H. 2021. Adsorption of Malachite Green Dye onto Mesoporous Natural Inorganic Clays: Their Equilibrium Isotherm and Kinetics Studies. Water, 13(7), 965.

70. Weber Jr, W.J., Morris, J.C. 1963. Kinetics of adsorption on carbon from solution. Journal of the Sanitary Engineering Division, 89(2), 31–59.

71. Zulfikar, M.A., Setiyanto, H., Djajanti, S.D. 2013. Effect of temperature and kinetic modelling of lignosulfonate adsorption onto powdered eggshell in batch systems. Songklanakarin Journal of Science & Technology, 35(3).